scientific reports

Check for updates

OPEN

Primate-specific 82-kDa choline acetyltransferase attenuates progression of Alzheimer's disease-like pathology in the APP^{NL-G-F} knock-in mouse model

Hadir E. AlQot & Rebecca Jane Rylett✉

Alzheimer's disease (AD) is characterized by amyloidosis, neuroinflammation, cholinergic dysfunction and cognitive impairment. In AD, the cholinergic neuronal marker choline acetyltransferase (ChAT) is reduced and the primate-specific nuclear isoform, 82-kDa ChAT, is mislocalized to cytoplasm. Cell-based studies suggest a role for 82-kDa ChAT in regulating expression of AD-related genes with potential reductions in β-amyloid (Aβ) levels. To study this further, we crossed transgenic mice expressing human 82-kDa ChAT with the AD mouse model APP^{NL-G-F} and used molecular techniques and neurobehavioral tests to study the impact of 82-kDa ChAT on AD pathology. These mice had altered expression of genes linked to Aβ clearance and inflammation, and reduced cognitive decline, amyloidosis and gliosis. These effects were inversely related to age and Aβ plaque load and correlated best with 82-kDa ChAT localized to nuclei of neurons. The study suggests a role for 82-kDa ChAT in decreasing AD-like pathology.

Keywords 82-kDa choline acetyltransferase, APP^{NL-G-F} mice, Alzheimer's disease, β-Amyloid clearance, Microglia, Neurobehavioral testing, PCR array, Immunofluorescence

Abbreviations

ABCA1	ATP binding cassette transporter A1
ACh	Acetylcholine
AD	Alzheimer's disease
Aβ	β-Amyloid
APP	Amyloid precursor protein
ApoA	Apolipoprotein A
ApoE	Apolipoprotein E
BACE	β-Secretase
BBB	Blood brain barrier
BCSFB	Blood cerebrospinal fluid barrier
ChAT	Choline acetyltransferase
ECE	Endothelin converting enzymes
IDE	Insulin degrading enzyme
Lrp1	Lipoprotein receptor-related protein 1
NEP	Neprilysin
NFT	Neurofibrillary tangles

Alzheimer's disease (AD) is an age-related neurodegenerative disease characterized by memory loss and cognitive dysfunction[1]. It accounts for 62% of dementia cases and is the seventh leading cause of death worldwide[2]. Globally, 51.6 million people live with AD and related dementias; the economic burden exceeds $2.8 trillion/year and is expected to triple in the next fifteen years[3].

Department of Physiology and Pharmacology, Schulich School of Medicine & Dentistry, Robarts Research Institute, University of Western Ontario, London, ON N6A 5K8, Canada. ✉email: jane.rylett@schulich.uwo.ca

AD pathology is characterized by intracellular neurofibrillary tangles (NFTs), β-amyloid (Aβ) plaques, dystrophic neurites and reactive gliosis with subsequent synaptic and neuronal loss in affected brain regions[1]. NFTs and plaques consist primarily of hyper-phosphorylated tau, a microtubule-associated protein[4], and Aβ, respectively[5]. Several hypotheses have been advanced to explain the etiology of AD, including cholinergic neuron dysfunction, tau propagation, inflammation and oxidative stress, neurovascular collapse and metabolic perturbations, but the Aβ hypothesis remains a leading focus driving development of therapeutics in clinical trials, including the anti-amyloid antibody therapies. Elevated Aβ levels, due either to increased production and/or reduced clearance, are considered early events in the pathology cascade of the disease[6].

Aβ production depends on sequential proteolysis of amyloid precursor protein (APP) by β-secretase (BACE1) and γ-secretase complex[5]. Alternatively, APP can undergo non-amyloidogenic metabolism by α-secretases, precluding production of Aβ. Under physiological conditions, Aβ is effectively cleared by several mechanisms, including uptake by glial cells[7], proteolytic cleavage[8] and systemic elimination by vascular[9] and lymphatic systems[10]. Cytosolic Aβ is degraded by the ubiquitin-proteasome system[11], lysosomal peptidases (cathepsins)[12] and metallo-endopeptidases, including insulin degrading enzyme (IDE), neprilysin (NEP) and endothelin converting enzymes (ECEs)[8]. Meanwhile, interstitial Aβ is cleared by (1) glial uptake (phagocytosis, pinocytosis, endocytosis) and cytosolic proteolysis[7], (2) extracellular degradation by neuron-/glia-derived proteases (IDE, NEP, ECEs, plasminogen activators/plasmin, angiotensin converting enzyme and matrix metalloproteinases 2,3 and 9)[8] or (3) vascular clearance to the periphery (by transporters in the blood brain barrier (BBB) and blood cerebrospinal fluid barrier (BCSFB))[9]. These clearance systems can be defective in AD and restoring their function can lead to reduced Aβ pathology and improved behavioral outcomes[13].

Several chaperones are important for Aβ elimination, including apolipoproteins E and A (ApoE and ApoA) and their clearance efficiency is dependent on the isoform (in the case of ApoE) and lipidation status[14]. The ATP-binding cassette transporter A1 (ABCA1) plays a crucial role in ApoE and ApoA lipidation, facilitating binding to Aβ and subsequent proteolytic degradation (IDE and NEP) in the extracellular space[15]. Additionally, lipidated ApoE/ApoA-Aβ complexes can be eliminated by uptake into either neuronal or glial cells[16] and/or drainage across the cerebral vasculature in a manner dependent on low density lipoprotein receptor-related protein 1 (Lrp1)[17].

The cholinergic neuronal system plays an important role in AD. Acetylcholine (ACh) can promote non-amyloidogenic processing of APP thereby reducing Aβ production, while high Aβ levels can suppress cholinergic neuron function[18]. Stimulation of microglial and neuronal nicotinic receptors leads to enhanced phagocytosis of Aβ[19] and reduced NFTs pathology, respectively. Additionally, cholinergic neuron dysfunction is linked to reduced vascular Aβ clearance (defective vasomotor tone in the BBB), neuroinflammation (compromised anti-inflammatory role of ACh[20]) and correlates to the late-onset AD risk factor ApoE4. Given their susceptibility to changes in neuronal microenvironment, cholinergic-rich brain regions (hippocampus, basal forebrain and striatum) are especially vulnerable to AD-related neurodegenerative changes[21]. Consequently, the activity and/or levels of several cholinergic markers, including the ACh synthesizing enzyme choline acetyltransferase (ChAT), are reduced in AD[22].

ChAT is a key cholinergic neuron marker that exists in several isoforms, including the primate-specific 82-kDa ChAT. With two strong nuclear localization signals, 82-kDa ChAT protein is localized primarily within the nucleus, but it is also found in cytoplasm of cholinergic neurons in necropsy brain of older persons or persons diagnosis with AD[23,24]. The function of 82-kDa ChAT in the nucleus is not fully understood, but it may have a role in cellular responses to stress, including Aβ, possibly by transcriptional and epigenetic regulation[25,26]. To elucidate actions of this form of ChAT, we developed a transgenic mouse model expressing human 82-kDa ChAT (Cre + ChAT+) and found that this recapitulated age-dependent expression and subcellular localization similar to that reported in humans[27]. In the current study, we cross-bred 82-kDa ChAT expressing mice with an AD mouse model ($APP^{NL\text{-}G\text{-}F/NL\text{-}G\text{-}F}$) resulting in generation of AD model mice expressing 82-kDa ChAT ($APP^{NL\text{-}G\text{-}F/WT}$ X Cre + ChAT+) to study the impact of expression of this ChAT protein in cholinergic forebrain neurons on AD-like pathology and progression.

Results

82-kDa ChAT and Aβ pathology

Immunofluorescence staining associated with Aβ was found to be reduced in cortex and hippocampus of brain sections prepared from $APP^{NL\text{-}G\text{-}F/WT}$ X Cre + ChAT + mice when compared to $APP^{NL\text{-}G\text{-}F/WT}$ mice. This effect was also seen, but to a lesser extent, in some subcortical areas. These changes were age-related, being greater at ages 6 and 12 months than at age 18 months (Fig. 1A–C). Quantification of Aβ immunofluorescence in cortex and hippocampus showed that at 6 and 12 months old, but not at 18 months old, $APP^{NL\text{-}G\text{-}F/WT}$ X Cre + ChAT + mice exhibit signtificantly lower amyloidosis compared to age-matched $APP^{NL\text{-}G\text{-}F/WT}$ control mice (mean difference ± SEM, 6 month old males: -1.37 ± 0.49, females: -1.50 ± 0.49, 12 month old males: -4.50 ± 1.53, females: -5.28 ± 1.79, $p \leq 0.05$, Fig. 1D-F). Age-dependent increases in Aβ immunfluorescence were noted, with higher Aβ immunfluorescence in older compared to younger mice. Moreover, sex differences were noted with Aβ immunfluorescence being greater in female mice relative to male mice, with this achieving statistical significance at age 18 months (Fig S1A). Changes in Aβ immunofluorescence imaging data was confirmed using ELISA to measure total $Aβ_{1\text{-}42}$ levels in the hippocampus of both control $APP^{NL\text{-}G\text{-}F/WT}$ mice and $APP^{NL\text{-}G\text{-}F/WT}$ X Cre + ChAT + mice (Fig. 1G). Importantly, total $Aβ_{1\text{-}42}$ levels were significantly lower in the hippocampus of $APP^{NL\text{-}G\text{-}F/WT}$ X Cre + ChAT + mice compared to control $APP^{NL\text{-}G\text{-}F/WT}$ mice at all ages tested ($p \leq 0.05$). While there was a trend towards $Aβ_{1\text{-}42}$ levels being higher in female $APP^{NL\text{-}G\text{-}F/WT}$ control mice compared to male $APP^{NL\text{-}G\text{-}F/WT}$ control mice, this only achieved statistical significance at age 6 months ($p \leq 0.05$), Fig S1B).

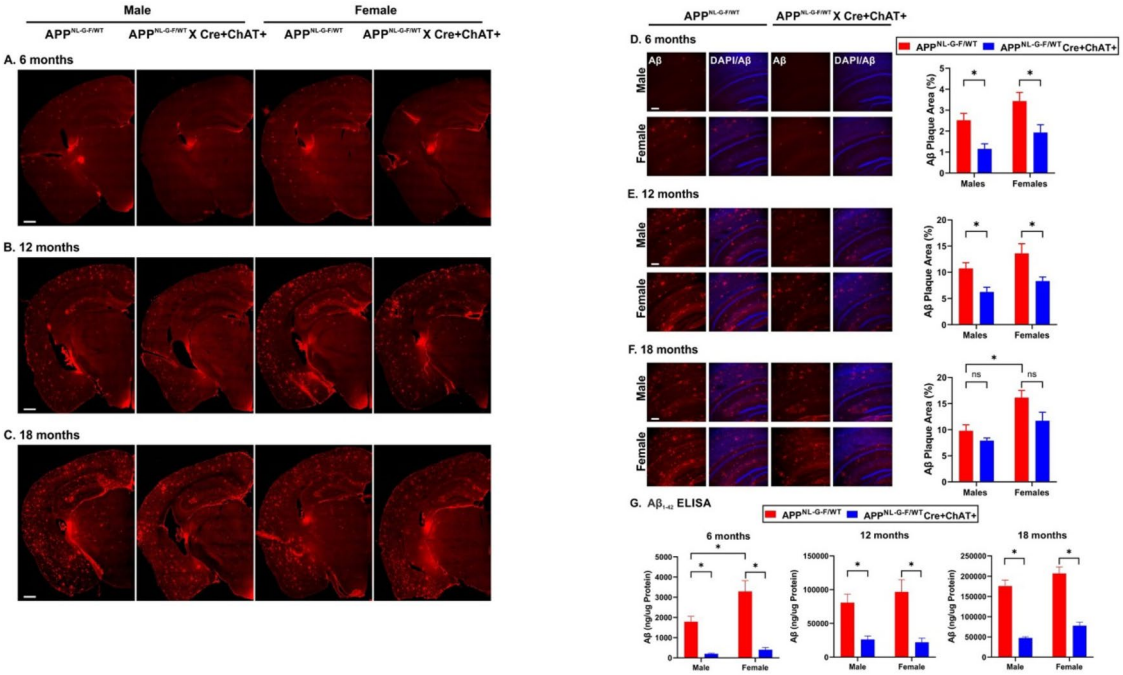

Fig. 1. Amyloidosis. Aβ deposition in brain of male and female $APP^{NL\text{-}G\text{-}F/WT}$ and $APP^{NL\text{-}G\text{-}F/WT}$ X Cre + ChAT + mice at ages of 6 (**A**), 12 (**B**) and 18 (**C**) months was detected in 40 µm thick coronal sections using Aβ antibody clone MOAB2. Heterozygous $APP^{NL\text{-}G\text{-}F/WT}$ mice expressing 82-kDa ChAT showed reduced Aβ immunofluorescence compared to control $APP^{NL\text{-}G\text{-}F/WT}$ not expressing 82-kDa ChAT, with this difference being less prominent with increasing age and Aβ load. All images were obtained with a 20× objective using a wide-field Thermo-Evos imaging system. Scale bars represent 500 µm ($n = 3$/age/sex/genotype). Representative confocal images and the corresponding quantification of Aβ-immunopositive signals in the hippocampus and cortex of $APP^{NL\text{-}G\text{-}F/WT}$ and $APP^{NL\text{-}G\text{-}F/WT}$ X Cre + ChAT + mice at ages of 6 (**D**), 12 (**E**) and 18 (**F**) months. Lower Aβ fluorescence is seen in 6 and 12 months old $APP^{NL\text{-}G\text{-}F/WT}$ X Cre + ChAT + mice compared to age-matched $APP^{NL\text{-}G\text{-}F/WT}$ control mice. A sex difference in Aβ deposition is noted in the $APP^{NL\text{-}G\text{-}F/WT}$ control mice at the oldest age (18 months), with females exhibiting higher amyloidosis compared to males. Images were acquired with a 10× objective using a Leica-TSC SP8 confocal microscope from a minimum of four different biological replicates for each age, sex and genotype. Scale bars represent 200 µm. Statistical analysis was performed using two-way ANOVA-Sidak, data are expressed as mean ± SEM, $^{*}p \leq 0.05$ ($n = 3$/age/sex/genotype). Total levels of $A\beta_{1\text{-}42}$ were measured by ELISA in the hippocampus of 6, 12, and 18 month old $APP^{NL\text{-}G\text{-}F/WT}$ and $APP^{NL\text{-}G\text{-}F/WT}$ X Cre + ChAT + mice (**G**). Significant reductions in hippocampal total $A\beta_{1\text{-}42}$ levels were observed in $APP^{NL\text{-}G\text{-}F}$ X Cre + ChAT + compared to age-matched control mice. $A\beta_{1\text{-}42}$ levels were normalized to total protein content. Statistical analysis was performed using two-way ANOVA-Sidak, $^{*}p \leq 0.05$, $n = 4$/sex/genotype/age.

82-kDa ChAT and microgliosis

Changes in microglial activation were investigated using the microglial marker Iba1. High power images of the cortex and hippocampus (Fig. 2) showed similar results for Aβ staining as described previously. Gliosis, as indicated by Iba1 immunofluorescence, appeared to increase in parallel with elevated Aβ deposition at ages 6, 12 and 18 months (Fig. 2A-C). Relative to $APP^{NL\text{-}G\text{-}F/WT}$ mice, qualitative decreases in Iba1 immunofluoresence were noted in in brain sections from $APP^{NL\text{-}G\text{-}F/WT}$ X Cre + ChAT + mice, suggesting potentially lower reactivity/gliosis consistent with reduced amyloidosis. This was more prominent at 6 and 12 months of age (Fig. 2A,B) than at 18 months of age (Fig. 2C).

Gene expression profiles in $APP^{NL\text{-}G\text{-}F/WT}$ and $APP^{NL\text{-}G\text{-}F/WT}$ X Cre + ChAT + mice

Based on these observed differences that were more evident at younger ages, we performed PCR arrays to assess possible changes in expression of genes related to Alzheimer's disease and inflammation in 6 month old mice.

Alzheimer's disease PCR array

Differential changes in gene expression were observed in $APP^{NL\text{-}G\text{-}F/WT}$ X Cre + ChAT + mice compared to $APP^{NL\text{-}G\text{-}F/WT}$ control mice on the AD PCR array, with 39 genes altered in both sexes (males: 35 upregulated and 4 downregulated, females: 38 upregulated and 1 downregulated, Table S1). Some of these genes were related to Aβ degradation (*Ide*, *Plat*, *Plau*, *Plg*), lipid metabolism/Aβ clearance (*Abca1*, *Apoa*, *Lpl*, *Lrp1*, *Lrp8*) and insulin signaling (*Ide*, *Insr*, *Igf2*) (Fig. 3A and C).

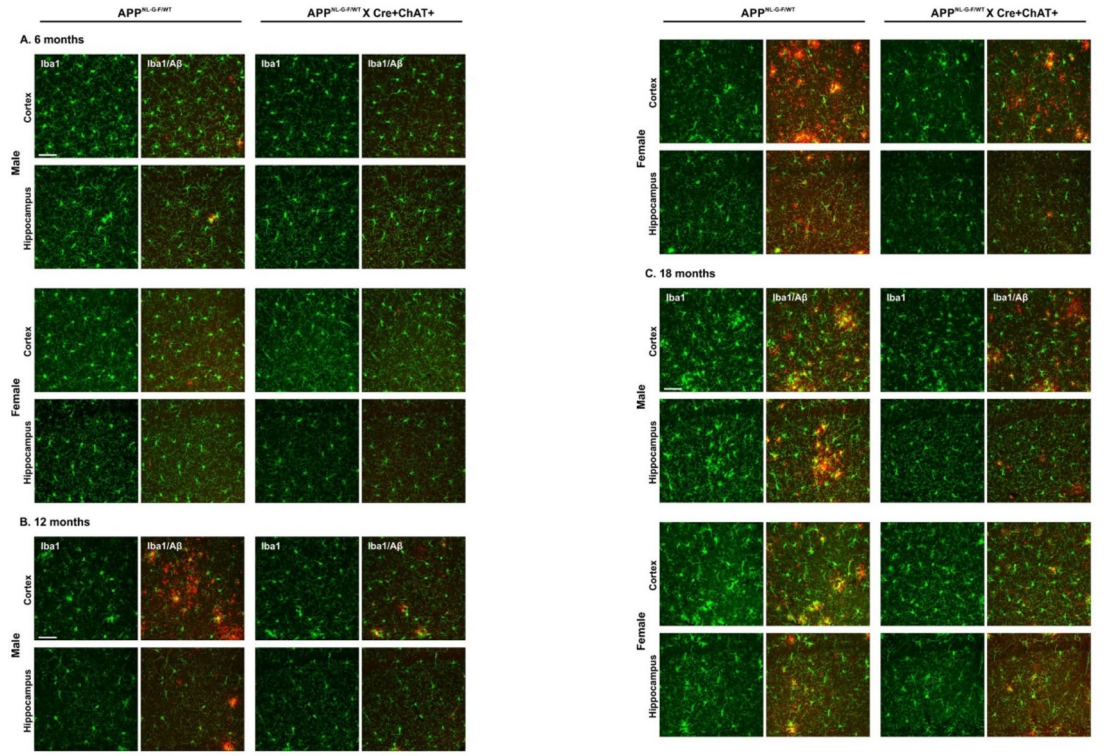

Fig. 2. Microgliosis. Consistent with the pattern of Aβ plaque deposition, differences in gliosis were observed between $APP^{NL\text{-}G\text{-}F/WT}$ and $APP^{NL\text{-}G\text{-}F/WT}$ X Cre + ChAT + mice, with this being more prominent in younger mice at 6 (**A**) and 12 (**B**) months of age and less evident in older mice at 18 months of age (**C**). Morphologically, microglia in the $APP^{NL\text{-}G\text{-}F/WT}$ mice appear more activated with larger amoeboid cell bodies, retracted and thicker branches compared to $APP^{NL\text{-}G\text{-}F/WT}$ X Cre + ChAT + mice. Images were acquired with a 40× objective using a Leica-TSC SP8 confocal microscope from at least four different biological replicates, with six fields/section, for each age, sex, and genotype (Green: Iba1, Red: Aβ). Scale bars represent 50 µm.

Chemokines and cytokines PCR array

Relative to control mice, $APP^{NL\text{-}G\text{-}F/WT}$ X Cre + ChAT + mice showed significant changes in 43 genes in males (36 upregulated and 7 downregulated) and 24 genes in females (22 upregulated and 2 downregulated) on the chemokines and cytokines PCR array (Table S2). Among these were genes related to pro-inflammatory markers (upregulated: *CCl20*, *Il12*, *Il17*, *Il18*, *Il23*; downregulated: *Ccl5*, *Ccl7*, *Cxcl10*, *Ifnγ*, *Il6*), anti-inflammatory markers (upregulated: *CCl2*, *CCl17*, *CCl22*, *CCl24 CCl24*, *Csf1 Il11*, *Il22*, *Il1rn*, *Tgfβ*, *Csf1*), growth factors (upregulated: *Bmps*, *Vegfa*, *Tgfβ*, *Osm*) and neuroprotective factors (upregulated: *Cxcl12*, *Cxcl16*, *Lif*, *spp1*) (Fig. 3B and D).

Factors involved in Aβ degradation/clearance

Based on results from the AD PCR array related to Aβ elimination, we validated changes in expression at the protein level of selected genes that play important roles in Aβ clearance[8,15–17], specifically ABCA1, LRP1 and IDE. Immunoblots showed that at ages 6 and 12 months $APP^{NL\text{-}G\text{-}F/WT}$ X Cre + ChAT + mice had significantly higher levels of ABCA1, IDE and LRP1 proteins in the cortex and hippocampus when compared to age-matched $APP^{NL\text{-}G\text{-}F/WT}$ control mice (Fig. 4A and B). At 18 months of age, these changes were more variable, often not achieving statistical significance (Fig. 4C).

Pro- and anti-inflammatory markers

We showed previously that mice expressing 82-kDa ChAT exhibit an altered inflammatory profile compared to age-matched wild-type mice[27]. In the current study, we extended this comparison to reveal that 82-kDa ChAT expressing AD model mice had changes in expression of gliosis and inflammation-related genes when compared to AD model mice not expressing 82-kDa ChAT. This was investigated using immunoblots to probe steady-state protein levels for the pro-inflammatory/anti-inflammatory marker pairs, iNOS/Arg1 and Cd86/Cd206. Compared to $APP^{NL\text{-}G\text{-}F/WT}$ control mice, 6 month old $APP^{NL\text{-}G\text{-}F/WT}$ X Cre + ChAT + mice had reduced Iba1, iNOS, Cd86 protein levels and increased Arg1 and Cd206 protein levels (Fig. 5A). At ages 12 and 18 months, Iba1 protein levels were unchanged while individual markers and/or ratios exhibited variable significance (Fig. 5B and C).

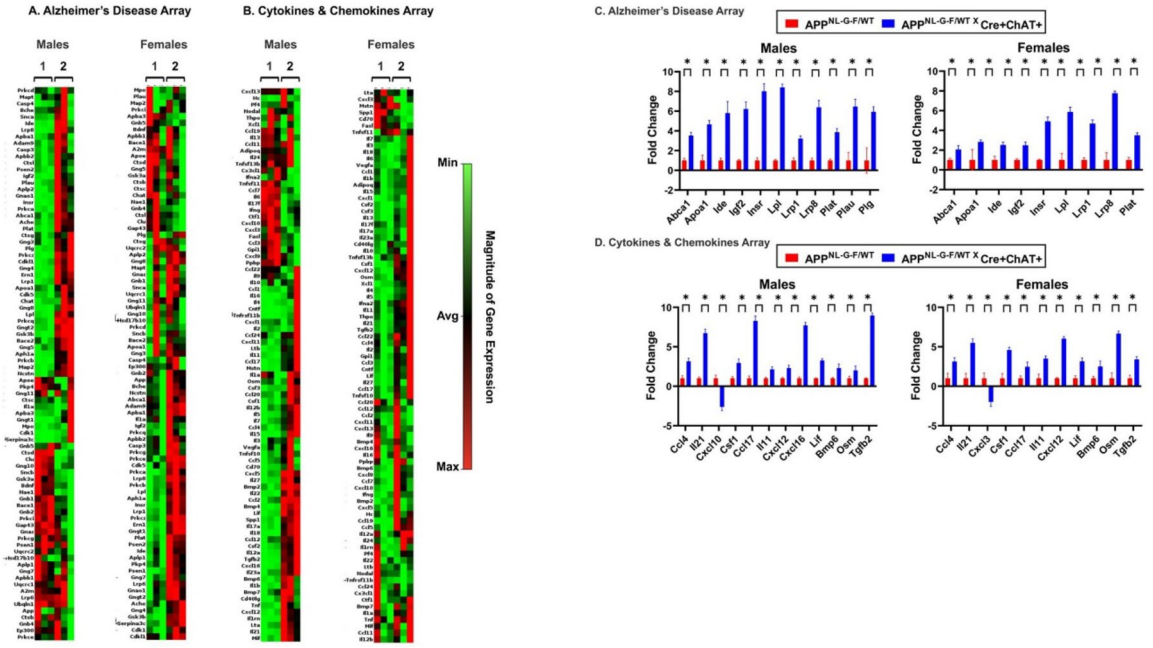

Fig. 3. RT2 Profiler™ PCR Arrays in 6 months old mice. Total hippocampal RNA was extracted from 3 independent biological replicates for each genotype and sex and was probed for changes in 84 genes implicated in Alzheimer's disease pathology (PAMM-057ZD) (**A**, **C**) and chemokines and cytokines pathways (PAMM-150ZD) (**B**, **D**). A cut-off of at least 2-fold change was set with a $p \leq 0.05$ and all genes were normalized to a panel of housekeeping genes. (**A**, **B**) Heat maps showing clusters of the relative expression of genes across all samples tested. Rows represent individual genes while columns represent individual biological samples. Group 1 represent control samples from $APP^{NL\text{-}G\text{-}F/WT}$ mice while Group 2 represents $APP^{NL\text{-}G\text{-}F/WT}$ X Cre + ChAT + mice. (**C**,**D**) histograms showing representative samples of genes with at least a 2-fold change in $APP^{NL\text{-}G\text{-}F/WT}$ X Cre + ChAT + mice relative to $APP^{NL\text{-}G\text{-}F/WT}$ control mice. Heat maps and fold-change analysis were performed using Geneglobe's online platform (RT^2 Profiler PCR Data Analysis). Data shown as fold change ± standard deviation (SD) was obtained from 3 independent experiments for each sex and genotype. Statistical analysis was performed using 2-way ANOVA-Sidak, $^*p \leq 0.05$.

Behavioral phenotyping of $APP^{NL\text{-}G\text{-}F/WT}$ and $APP^{NL\text{-}G\text{-}F/WT}$ X Cre + ChAT + mice

Habituation and general activity

At all ages tested, male and female $APP^{NL\text{-}G\text{-}F/WT}$ and $APP^{NL\text{-}G\text{-}F/WT}$ X Cre + ChAT + habituated normally to the open-field arena without significant differences between the genotypes (Fig S4A). General and exploratory activity assessed by analyzing the initial 10 min of the first day in the habituation session showed that 12 and 18 month old $APP^{NL\text{-}G\text{-}F/WT}$ X Cre + ChAT + male mice were significantly more active than $APP^{NL\text{-}G\text{-}F/WT}$ control male mice (mean difference ± SEM, 1.89 ± 0.62 and 1.75 ± 0.66, $p \leq 0.05$, respectively, Fig. 6A). Furthermore, 6 month old female $APP^{NL\text{-}G\text{-}F/WT}$ X Cre + ChAT + mice were more anxious when compared to the $APP^{NL\text{-}G\text{-}F/WT}$ female control mice, spending less time at the margin and more time at the center of the arena (mean difference ± SEM, 1.45 ± 0.61 and 1.64 ± 0.42, $p \leq 0.05$, Fig. 6A).

Forelimb strength and weight

No differences were observed in grip strength between genotypes at either 6, 12 or 18 months of age (Fig S4B). Significant genotype effects were observed in body weight at 18 months of age (Fig. 6B), with $APP^{NL\text{-}G\text{-}F/WT}$ X Cre + ChAT + mice weighing significantly less than $APP^{NL\text{-}G\text{-}F/WT}$ mice (mean difference ± SEM, males: -8.89 ± 2.95, $p \leq 0.05$, females: -6.76 ± 1.58, $p \leq 0.05$).

Learning and memory

Spatial learning, assessed during the training phase in the Barnes maze (Fig. 6C, S4C) and Morris water maze (Fig. 6D, S4D), showed that all mice acquired the task as indicated by the reduced number of errors, distance travelled and time to locate the escape target. In the Barnes maze, 12 month old female $APP^{NL\text{-}G\text{-}F/WT}$ mice had reduced learning compared to $APP^{NL\text{-}G\text{-}F/WT}$ X Cre + ChAT + mice with significantly longer escape latencies on days 3 and 4 (mean difference ± SEM, 34.8 ± 9.0 and 27.6 ± 6.7, $p \leq 0.05$, respectively, Fig. 6C). Short- and long-term memory were assessed on days 5 and 12 (24 h and one week after the last training session, respectively) of the Barnes maze and Morris water maze. Differential effects were observed, with better performance at the youngest age and in the first probe trial (Fig. 6C and D). At 6 months of age, all mice were able to recall the target location during the first probe trial, with higher target visit preference/duration. In the second probe trial, a similar pattern was observed for all mice except that female $APP^{NL\text{-}G\text{-}F/WT}$ mice failed to distinguish the target location. At 12 months of age, and only in the Barnes maze, $APP^{NL\text{-}G\text{-}F/WT}$ mice showed reduced target visits

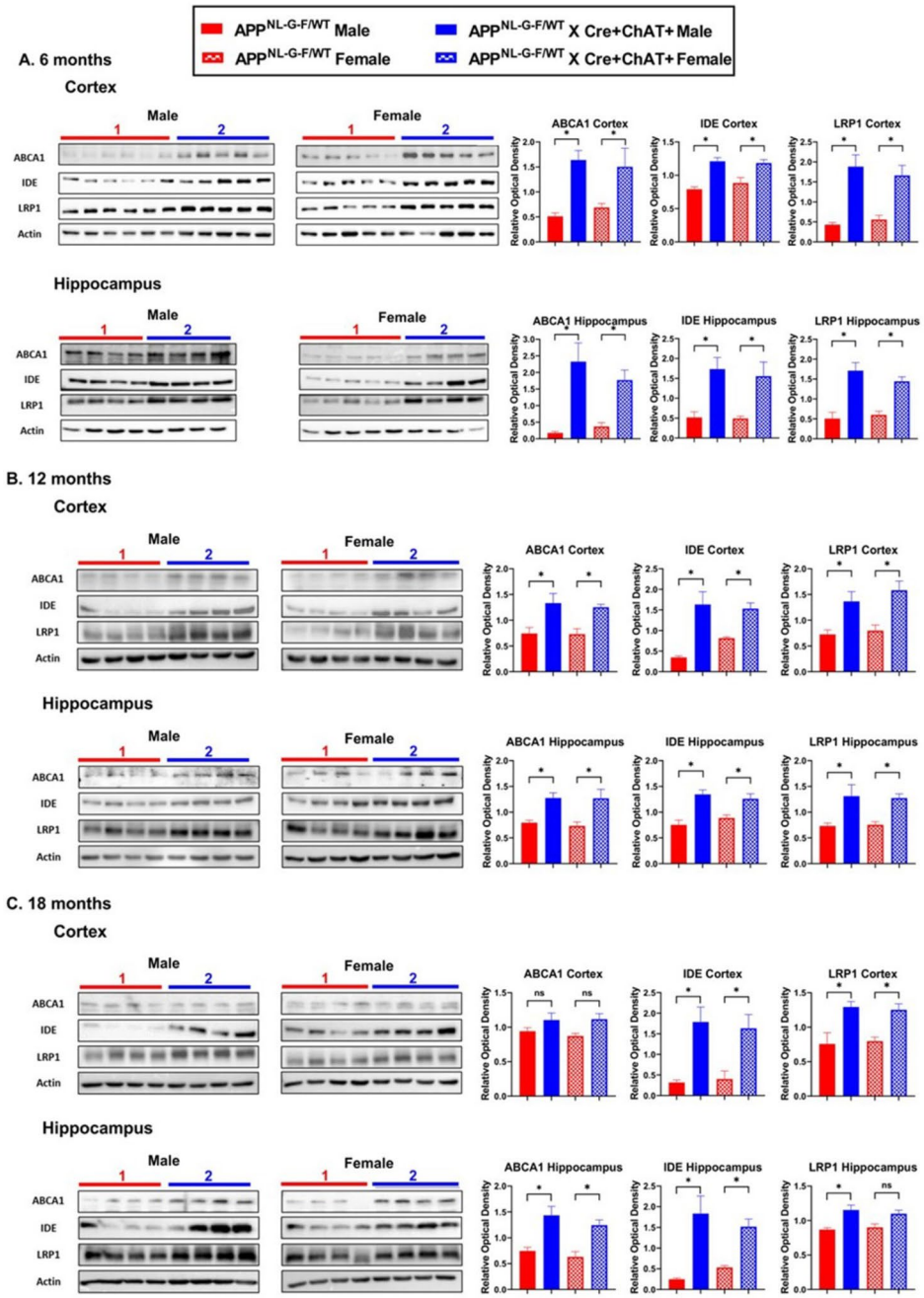

Fig. 4. Clearance and Aβ degradation. Proteins in cortical and hippocampal lysates (25 µg) were separated using 8% SDS-PAGE, then transferred and probed with antibodies against target proteins. Representative immunoblots and densitometric analysis of ABCA1, IDE and LRP1 in 6 (**A**), 12 (**B**) and 18 (**C**) month old mice. Red (1) and blue (2) lines indicate lanes with samples from $APP^{NL\text{-}G\text{-}F/WT}$ and $APP^{NL\text{-}G\text{-}F/WT}$ X Cre + ChAT + mice, respectively. Increased immunoreactivity for all proteins was observed in $APP^{NL\text{-}G\text{-}F/WT}$ X Cre + ChAT + compared to $APP^{NL\text{-}G\text{-}F/WT}$ mice, at age 6 (**A**) and 12 (**B**) months and to a lesser extent at age 18 (**C**) months. Statistical analysis was performed using one-way ANOVA-Sidak, data are expressed as mean ± SEM, $^*p \leq 0.05$ ($n = 4$–6/age/sex/genotype). Full length (uncropped) immunoblots are provided in Supplementary Fig. S3 for the (**A**) 6, (**B**) 12 and (**C**) 18 month ages.

and duration whereas $APP^{NL\text{-}G\text{-}F/WT}$ X Cre + ChAT + mice maintained good target recall with the female mice having significantly higher target frequency relative to $APP^{NL\text{-}G\text{-}F/WT}$ females (mean difference ± SEM, 2.6 ± 0.7, $p \leq 0.05$, Fig. 6C, S4C). At 18 months of age, only mice expressing the $APP^{NL\text{-}G\text{-}F/WT}$ X Cre + ChAT + genotype retained effective recall in the first trial whereas in the second trial both genotypes and sexes failed to retain the target location showing decreased target visits and duration below chance (Fig. 6C and D).

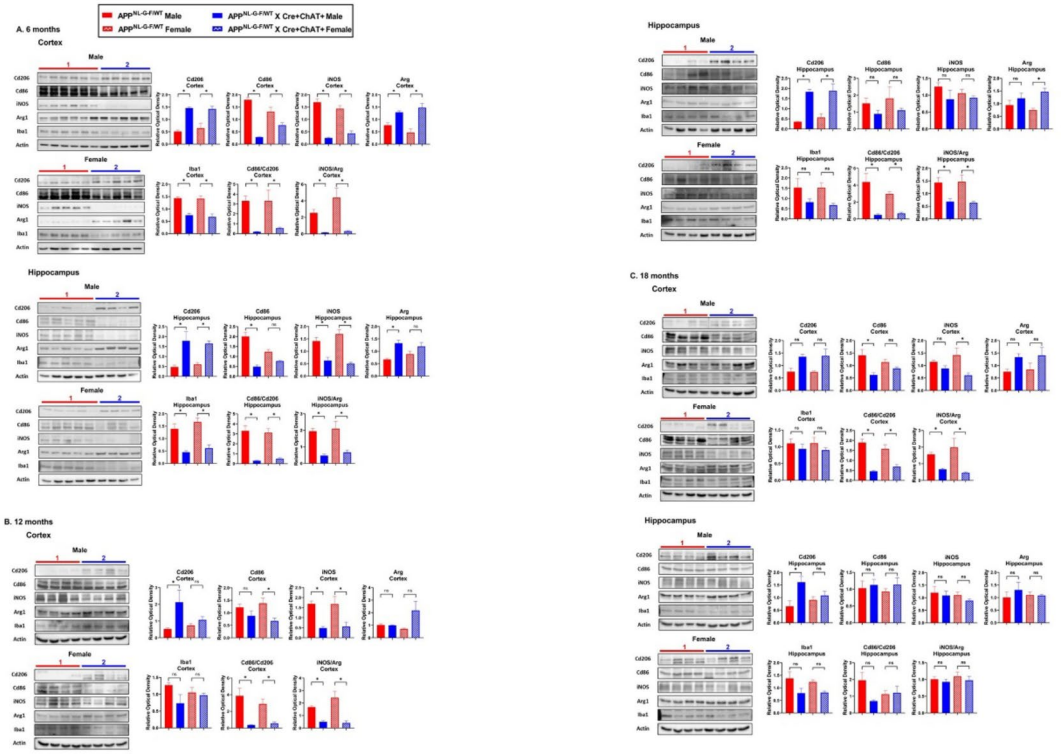

Fig. 5. Pro-inflammatory and anti-inflammatory markers. Immunoblots were performed to determine steady-state protein levels of the microglial marker Iba1 and pro- (iNOS, Cd86) and anti-inflammatory (Arg1, Cd206) markers in cortex and hippocampus of $APP^{NL\text{-}G\text{-}F/WT}$ and $APP^{NL\text{-}G\text{-}F/\ WT}$ X Cre + ChAT + mice, at ages 6 (**A**), 12 (**B**) and 18 (**C**) months of age. Tissue lysates (25 µg) were separated using 8 or 12% SDS-PAGE, then transferred to PVDF membranes and probed with antibodies against target proteins. Red (1) and blue (2) lines indicate lanes with samples from $APP^{NL\text{-}G\text{-}F/WT}$ and $APP^{NL\text{-}G\text{-}F/WT}$ X Cre + ChAT + mice, respectively. Increased levels of the anti-inflammatory markers (Arg1 and Cd206), and lower levels of the microglial marker Iba1 and pro-inflammatory markers (iNOS and Cd86) were observed in $APP^{NL\text{-}G\text{-}F/WT}$ X Cre + ChAT + compared to $APP^{NL\text{-}G\text{-}F/WT}$ mice at 6 months of age (**A**), but not at 18 months of age (**C**). Moreover, elevated pro-inflammatory/anti-inflammatory ratios were found in control mice compared to mice expressing 82-kDa ChAT, an effect that decreases with age becoming non-significant at age 18 months. Immunopositive bands from 4, 5 or 6 biological replicates/age/sex/genotype were analyzed using densitometry and all samples were normalized to the loading control β-actin. Statistical analysis was performed using one-way ANOVA-Sidak, data are expressed as mean ± SEM, $^{*}p \leq 0.05$. Full length (uncropped) immunoblots are provided in Supplementary Fig. S2 for the (**A**) 6, (**B**) 12 and (**C**) 18 months ages.

Subcellular localization of 82-kDa ChAT

Using our antibody that recognizes the N-terminus of human 82-kDa ChAT, we observed immunopositive signals in $APP^{NL\text{-}G\text{-}F/WT}$ X Cre + ChAT + but not $APP^{NL\text{-}G\text{-}F/WT}$ mice, with this localized to both nucleus and cytoplasm of neurons at age 6 months and to a lesser extent at age 12 months (Fig. 7A and B). At age 18 months, immunofluorescence for 82-kDa ChAT was found to be localized primarily to the cytoplasm (Fig. 7C).

Discussion

The impact of expression of 82-kDa ChAT on AD-like pathology was studied by crossing the Cre + ChAT + transgenic mouse developed in our laboratory[27] with the $APP^{NL\text{-}G\text{-}F/NL\text{-}G\text{-}F}$ AD model mouse[28]. The resulting $APP^{NL\text{-}G\text{-}F/WT}$ X Cre + ChAT + mice exhibited attenuated pathology and improved behavioral profile compared to $APP^{NL\text{-}G\text{-}F/NL\text{-}G\text{-}F}$ mice in an age-dependent manner. Critical differences included that $APP^{NL\text{-}G\text{-}F/WT}$ X Cre + ChAT + mice had significantly reduced cortical and hippocampal Aβ levels, decreased plaque pathology and reduced inflammation, consistent with reports for Aβ-lowering treatments[29]. This is consistent with, and extends to an in vivo model, our report that 82-kDa ChAT expression reduced release of Aβ from cortical neuron cultures from APP/PS1 AD model mice[25].

Interestingly, reduced Aβ plaques and gliosis observed in the $APP^{NL\text{-}G\text{-}F/WT}$ X Cre + ChAT + mice were greater at younger compared to older age. This suggests that the effects of 82-kDa ChAT expression had a greater impact on earlier stages of development of AD-like pathology in this mouse model. Since Aβ plaque accumulation is attributed to disturbed Aβ homeostasis[30], altered APP processing and/or enhanced Aβ clearance may underlie the reduction observed in $APP^{NL\text{-}G\text{-}F/WT}$ X Cre + ChAT + mice. Reduced Aβ level in neurons cultured from APP/PS1 mice transduced to express 82-kDa ChAT was accompanied by reduced expression of genes involved in

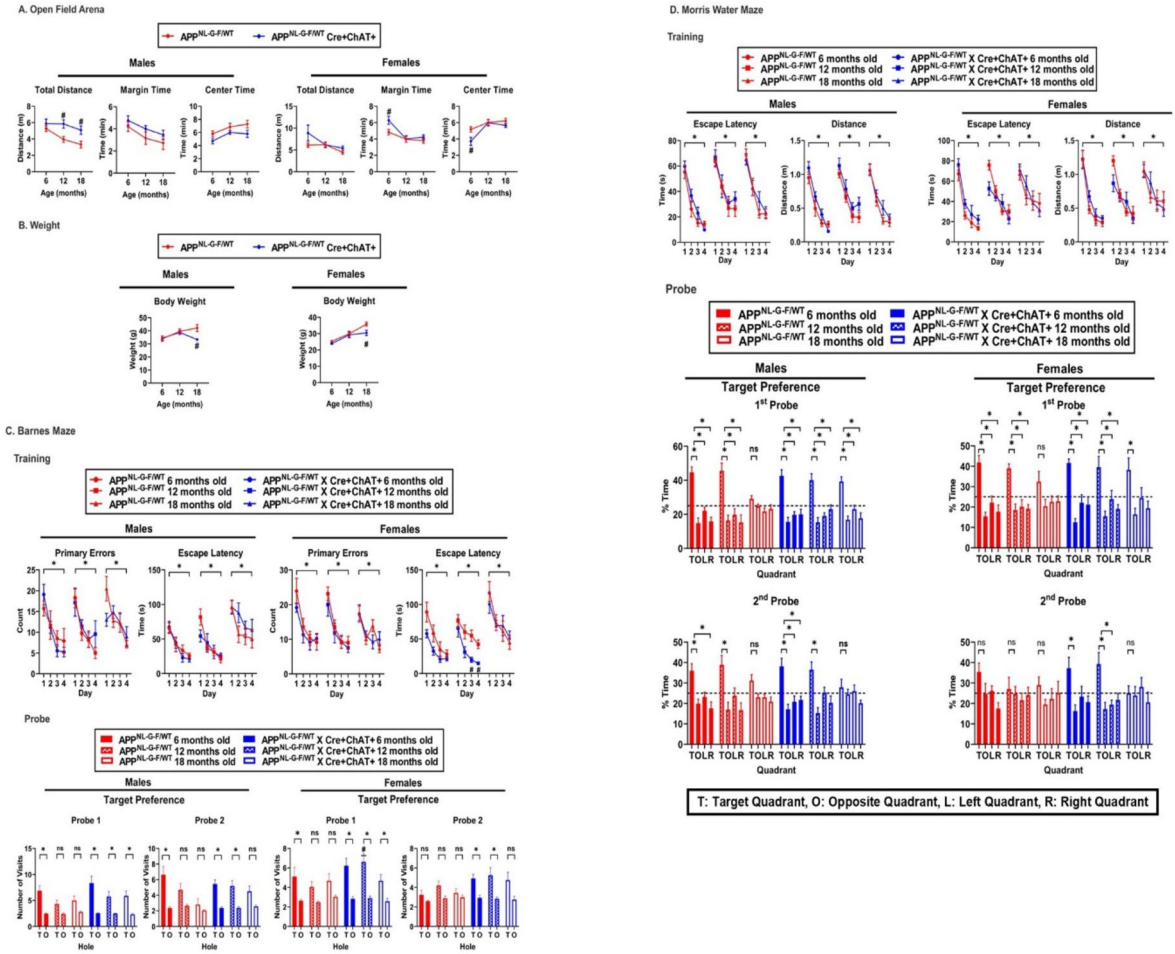

Fig. 6. Behavioral profiling. (**A**) General activity and exploratory behavior were assessed using activity recordings from the first session of the open field test (initial 10 min interval of the first day). At age 6 months, $APP^{NL\text{-}G\text{-}F/WT}$ X Cre + ChAT + female mice appeared to spend more time at the margin and less time at the center of the arena relative to $APP^{NL\text{-}G\text{-}F/WT}$ female mice (anxiogenic behavior). At ages 12 and 18 months, $APP^{NL\text{-}G\text{-}F/WT}$ X Cre + ChAT + male mice show increased locomotor activity compared to $APP^{NL\text{-}G\text{-}F/WT}$ male mice. Data are represented as mean ± SEM, $^{*}p \leq 0.05$, two-way ANOVA-Sidak, $n = 8$/age/genotype/sex. (**B**) Mice were weighed with no differences found between the genotypes at 6 and 12 months of age. At age 18 months, both male and female $APP^{NL\text{-}G\text{-}F/WT}$ X Cre + ChAT + mice weighed significantly less than $APP^{NL\text{-}G\text{-}F/WT}$ mice. Data are represented as mean ± SEM, $^{*}p \leq 0.05$, two-way ANOVA-Sidak, $n = 8$/age/sex/genotype. Learning and memory performance were assessed during training and probe phases, respectively, of the Barnes maze (**C**) and Morris water maze (**D**). During the training sessions of both mazes, all mice learned the target location effectively as indicated by the decrease in errors, distance and escape latency over the 4 days. In the Barnes maze, 12 month old $APP^{NL\text{-}G\text{-}F/WT}$ female mice appear to be learning at a slower rate relative to $APP^{NL\text{-}G\text{-}F/WT}$ X Cre + ChAT + female mice as indicated by the upward shift in the curve. In the probe trials (Probe 1/short term at day 5; Probe 2/long-term at day 12), reference memory is intact in both genotypes at ages 6 and 12 months as indicated by the higher target preference compared to non-target locations. However, at age 18 months, only the $APP^{NL\text{-}G\text{-}F/WT}$ X Cre + ChAT + mice maintain effective target recall for the short-term memory trial, whereas all mice fail to show significant target preference during the long-term trial. Data are represented as mean ± SEM, *time effect, $^{\#}$genotype effect, $^{*}p \leq 0.05$, two-way RM ANOVA-Tukey (training) and two-way ANOVA-Sidak (Probe), $n = 8$/age/genotype/sex.

amyloidogenic processing of APP[25,26]. The mechanism by which 82-kDa ChAT induces these genetic alterations are unknown, but molecular studies in our laboratory suggest either transcriptional or epigenetic changes[26]. In the present study, PCR arrays revealed differential changes in gene expression between experimental $APP^{NL\text{-}G\text{-}F/WT}$ X Cre + ChAT + and control $APP^{NL\text{-}G\text{-}F/WT}$ mice, some of which were observed in previous cell culture studies (*Aplp1*, *Aplp2*, *Apba1/Mint1/x11alpha*, *Adam9*)[25,26] with other novel findings emerging in the current animal model study (*Plat*, *Plau*, *Plg*, *Ide*, *Ir*, *Igf-2*, *Lrp1*, *Lrp6*, *Lrp8*, *Apoa1*, *Lpl*, *Abca1*, *Il11*, *Il12*, *Il22*, *Il23*, *Il6*, *Ifnγ*, *Cxcl12*, *Cxcl16*, *Bmps*, *Lif*, *Tgfβ*). Several of these genes are implicated in or have roles in AD-related pathways, including APP metabolism, insulin signaling, lipid transport or metabolism, inflammation, and some can be regulated by cholinergic transmission or are linked to the cholinergic neuron hypofunction observed in

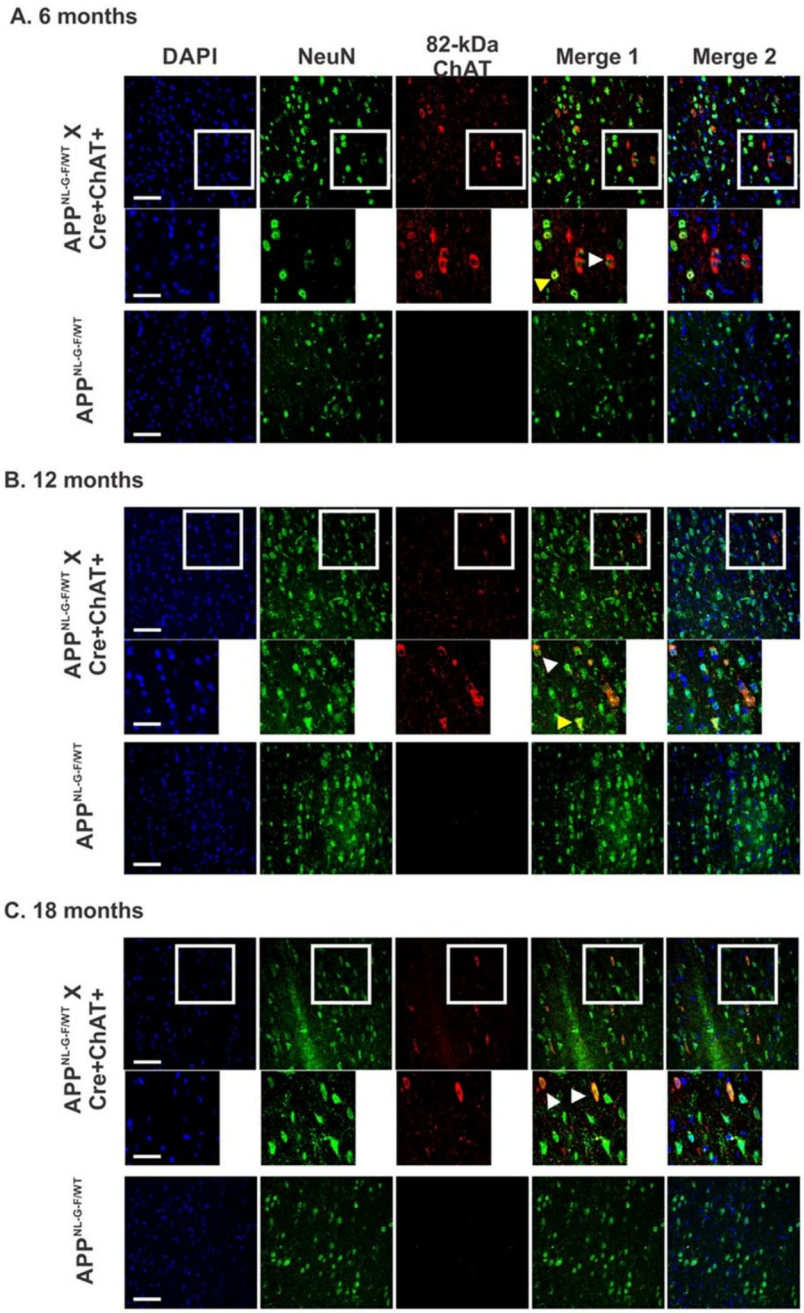

Fig. 7. 82-kDa ChAT immunofluorescence in basal forebrain medial septal nuclei. Free floating coronal sections, 40 µm in thickness, obtained from 6 (**A**), 12 (**B**) and 18 (**C**) month old $APP^{NL\text{-}G\text{-}F/WT}$ and $APP^{NL\text{-}G\text{-}F/WT}$ X Cre + ChAT + mice were stained using the N-terminal specific ChAT antibody (NTab). Immunopositive signals for 82-kDa ChAT protein were observed in basal forebrain neurons of $APP^{NL\text{-}G\text{-}F/WT}$ X Cre + ChAT + mice, but not in sections from $APP^{NL\text{-}G\text{-}F}$ mice. At the younger ages of 6 and 12 months, differential subcellular staining was noted with some neurons exhibiting nuclear signals for 82-kDa ChAT (red) with co-localization neuronal nuclear marker NeuN (green) (yellow arrows), whereas other neurons showed cytoplasmic fluorescence for 82-kDa ChAT (white arrows). By comparison, older mice (age 18 months) showed neurons with predominantly cytoplasmic staining for 82-kDa ChAT (white arrows). Images were obtained with a 40× objective using a Leica-TSC SP8 confocal microscope from at least four different biological replicates. Square insets have a zoom-in factor of 2× (Blue: DAPI, Green: NeuN, Red: 82-kDa ChAT, Merge 1: NeuN/82 kDa-ChAT, Merge 2: NeuN/82 kDa-ChAT/DAPI). Scale bars represent 50 µm and 25 µm for the magnified insets ($n = 3$/age/sex/genotype).

AD[31,32]. Other genes are important for cholinergic neuron function (*Bmps*)[33] and neuron-glia crosstalk (*CxCl12 and CxCl16*)[34] under normal or pathological conditions.

Based on PCR array data, the decreased AD-like pathology and progression observed in $APP^{NL\text{-}G\text{-}F/WT}$ X Cre + ChAT + mice may be attributed in part to reduced amyloidogenic processing of APP, increased Aβ elimination or improved inflammatory milieu. Within the scope of the current study, we selected three proteins that have a critical role in Aβ clearance, ABCA1, LRP1 and IDE, for more indepth analysis. The transcripts for these proteins were found to be elevated in the PCR array analysis of $APP^{NL\text{-}G\text{-}F/WT}$ X Cre + ChAT + mice, with these changes tending to be inversely related to the age of the mice and their Aβ plaque load. Enhanced expression of ABCA1 may promote lipidation of ApoE and/or ApoA1, leading to increased binding of Aβ to the lipoproteins[35]. The resultant apolipoprotein-Aβ complexes can reduce or prevent Aβ aggregation and plaque deposition[36] while facilitating extracellular proteolysis of Aβ[15]. This effect could be augmented further by elevated IDE levels in $APP^{NL\text{-}G\text{-}F/WT}$ X Cre + ChAT + mice related to increased Aβ degradation. Moreover, upregulated LRP1 can increase LRP1-mediated uptake of lipid-rich apolipoprotein-Aβ complexes into neurons and microglia or across the BBB and BCSFB where Aβ could undergo intracellular proteolysis or systemic elimination[37], respectively.

Microglial cells have critical roles in Aβ clearance[7] and changes in microglial activation and their contribution to pathology is well documented for AD[38]. Microglia can adopt either a protective or a pro-inflammatory phenotype to resolve pathology, but at more advanced disease stages they acquire a chronic pro-inflammatory state that aggravates pathology[38]. Promoting the former phenotype could enhance Aβ clearance and slow disease progression[39]. Based on apparent alterations in gliosis and cytokines/chemokines-related genes in $APP^{NL\text{-}G\text{-}F}$ X Cre + ChAT + mice, coupled with previous observations in Cre + ChAT + mice inflammatory profile[27], we investigated changes in protein levels of pro-inflammatory (Cd86, iNOS) and anti-inflammatory markers (Cd206, Arg1) implicated in modifying AD pathology. Ratios of Cd86/Cd206 and iNOS/Arg1 are commonly used to phenotype microglia and the inflammatory environment[40] and both were reduced in young $APP^{NL\text{-}G\text{-}F}$ X Cre + ChAT + mice compared to control mice, suggesting a more anti-inflammatory environment. In relation to microglia, increased expression of Cd206 and Arg1 and decreased levels of Cd86 and iNOS are associated with anti-inflammatory/neuroprotective rather than pro-inflammatory phenotypes[40]. Interferon-γ[41], which is downregulated in $APP^{NL\text{-}G\text{-}F}$ X Cre + ChAT + mice, promotes proinflammatory microglia, whereas TGF-β[42] and CxCl16[43], which are upregulated in $APP^{NL\text{-}G\text{-}F}$ X Cre + ChAT + mice, shifts microglia to the neuroprotective-state. Thus, 82-kDa ChAT expression may have promoted an environment favoring neuroprotective microglia leading to enhanced Aβ clearance. This hypothesis requires further investigation because, whereas Cd86/Cd206 are immune-cell specific, iNOS/Arg1 can also derive from neurons. Importantly, reduced microgliosis in $APP^{NL\text{-}G\text{-}F}$ X Cre + ChAT + mice signifies a potential role for 82-kDa ChAT in promoting cholinergic neuron-glial crosstalk whereby improved cholinergic function leads to blunted glial activation and vice versa[44–46].

Of note, we observed some sex-dependent differences in the accumulation of Aβ plaques, specifically for mice in the $APP^{NL\text{-}G\text{-}F/WT}$ control group with female mice having higher levels compared to male mice. Sex differences have been found in AD patients with females having a higher incidence of disease and increased severity and rate of progression[47], although this is not seen consistently in all mouse models of AD[48]. While the mechanisms resulting in this sex difference have not been elucidated, they may be attributed to an underlying biological dimorphism observed in neuronal, vascular and immune responses[47].

Reduced plaque and inflammation-related pathology could underlie the improved neurobehavioral phenotype of $APP^{NL\text{-}G\text{-}F/WT}$ X Cre + ChAT + compared to control $APP^{NL\text{-}G\text{-}F/WT}$ mice. Young $APP^{NL\text{-}G\text{-}F/WT}$ X Cre + ChAT + mice exhibited anxiogenic traits with memory retention while older mice were leaner and hyperactive with anxiolytic behavior and improved short-term memory compared to age-matched $APP^{NL\text{-}G\text{-}F/WT}$ mice. To our knowledge, this is the first behavioral study conducted on heterozygous $APP^{NL\text{-}G\text{-}F/WT}$ mice and, based on their later onset of pathology compared to homozygous mice[28], behavioral alterations are expected to follow a similar temporal delay, resembling younger homozygous mice. In the absence of defective habituation and age-dependent hypoactivity, older $APP^{NL\text{-}G\text{-}F/WT}$ X Cre + ChAT + mice appear more active relative to $APP^{NL\text{-}G\text{-}F/WT}$ control mice. This could indicate an improved behavioral trait because while activity in $APP^{NL\text{-}G\text{-}F/NL\text{-}G\text{-}F}$ appears inconsistent (hyper-[49], hypo-[50] and unaltered[51,52]), younger 6 month old mice (with pathology and possibly behavior comparable to old $APP^{NL\text{-}G\text{-}F/WT}$) reliably show reduced activity[50]. Here, anxiety was unchanged in $APP^{NL\text{-}G\text{-}F/WT}$ mice and decreased in $APP^{NL\text{-}G\text{-}F/WT}$ X Cre + ChAT + with increasing age. Homozygous $APP^{NL\text{-}G\text{-}F/NL\text{-}G\text{-}F}$ mice exhibit mostly anxiolytic behavior[52,53] often linked to reduced inhibition due to plaque pathology and cholinergic dysfunction[54]. Hence, increased anxiety in young $APP^{NL\text{-}G\text{-}F/WT}$ X Cre + ChAT + mice compared to control mice may suggests an intact inhibition machinery given the reduced plaque pathology in the former group. As $APP^{NL\text{-}G\text{-}F/WT}$ X Cre + ChAT + mice age, anxiety levels decrease, paralleling increased plaque pathology and equates to the levels of $APP^{NL\text{-}G\text{-}F/WT}$ control mice.

Hippocampal-dependent spatial reference memory is among the first domains that decline in AD, and its dysfunction was modelled in $APP^{NL\text{-}G\text{-}F/NL\text{-}G\text{-}F}$ mice starting at age 6 months[55]; some reports show earlier (age 4 months)[56] or later (age 8 and 12 months)[51,57] onset of memory change in $APP^{NL\text{-}G\text{-}F/NL\text{-}G\text{-}F}$ mice. In the present study, $APP^{NL\text{-}G\text{-}F/WT}$ mice showed age-dependent memory decline, initially in long-term and subsequently in short-term retention, evident in the Barnes maze prior to the Morris water maze. Previous studies, using different murine AD models, demonstrated similar results where long-term memory decline preceded short-term retention deficits[58], and where dysfunction was apparent in one maze but not the other[28,59]. Interestingly, $APP^{NL\text{-}G\text{-}F/WT}$ X Cre + ChAT + mice showed a slower rate of decline in retention, maintaining intact short-term memory with a deficit only in long-term domain and solely in older mice. Moreover, consistent with human AD[60], female mice were more sensitive to cognitive impairment, presenting with an earlier onset compared to male mice. Studies using $APP^{NL\text{-}G\text{-}F/NL\text{-}G\text{-}F}$ mice did not consistently reveal sex differences in cognitive deficits, showing either greater dysfunction in female mice[52] or no sex difference[56]. Discrepancies in behavioral

phenotyping across studies can arise due to variability in experimental factors, including housing, environmental enrichment, experimental set-up, maze type, time of day, sex or age of animals and experimenter's age[61].

The subcellular localization of 82-kDa ChAT in the $APP^{NL\text{-}G\text{-}F}$ X Cre + ChAT + mice was also noted. We found in previous studies[27] that while 82-kDa ChAT is located predominately in basal forebrain neuronal nuclei in young Cre + ChAT + mice, this protein becomes mostly cytoplasmic in neurons in older mice. These data recapitulate findings for age-related changes in subcellular localization of 82-kDa ChAT in basal forebrain cholinergic neurons in necropsy human brain and that 82-kDa ChAT was localized primarily to neuronal cytoplasm in necropsy brain of patients diagnosed with MCI or early AD[24]. In the present studies with $APP^{NL\text{-}G\text{-}F}$ X Cre + ChAT + mice, 82-kDa ChAT protein showed varying degrees of nuclear and cytoplasmic distribution. Young mice with lower Aβ plaque load showed both nuclear and cytosolic localization of 82-kDa ChAT, contrasting with the mainly cytosolic pattern evident in older mice with higher Aβ plaque load that closely resembled data from aged Cre + ChAT + mice[27].

Nuclear localization of 82-kDa ChAT has been found to be critical to its biological impact as determined in cell-based studies. We identified that a nuclear localization sequence (NLS) in the first 9 amino acid residues of the N-terminus of human 82-kDa ChAT is critical for its translocation into the nucleus[23]. We also demonstrated that 82-kDa ChAT binds to specific sequence elements in DNA in nuclei of cells and that this localization and gene expression patterns are modified by cellular stress[26]; it was determined in these studies that changes in the association of 82-kDa ChAT with specific genes could play a role in the response of neural cells to stress[26]. It was also discovered in separate studies using a mutant form of 82-kDa ChAT that it is not necessary that the enzyme be catalytically active to affect expression of several genes, including some involved in amyloidogenic processing of APP[25]. The mechanisms regulating subcellular localization and nuclear translocation of 82-kDa ChAT have not been fully elucidated, but it could relate to its post-translational modification such as by phosphorylation[47,48,62] or to perturbations in the nuclear core complex and/or nucleocytoplasmic shuttling[63] as reported for some transcription and epigenetic factors in AD[64,65].

A limitation of the current studies is that the sample size for some approaches, particularly the behavioral analysis, was restricted by the complexity of the breeding required to obtain the correct genotypes. Experimental mice were required to have three independent transgenes (82-kDa ChAT, Cre and $APP^{NL\text{-}G\text{-}F}$) and could only be obtained through cross-breeding single transgenic lines on heterozygous backgrounds for two of these transgenes (Cre and 82-kDa ChAT). Thus, the yield of the target genotype was low and time-consuming. However, these studies are critical as they produced much needed information required to assess the impacts of neuronal expression of human 82-kDa ChAT in vivo on progression of AD-like pathology. Future experiments could focus on validating the effect of 82-kDa ChAT on inflammation and the neuron-glial axis and dissecting the underlying mechanisms, as well as assessing potential paths for maintaining expression of 82-kDa ChAT in cholinergic neurons at older ages.

In conclusion, this is the first report of the Cre + ChAT + transgenic mouse model in studies of the impact of 82-kDa ChAT on AD-like pathology. Expression of 82-kDa ChAT in brain of AD model mice slowed progression of AD-like pathology potentially by upregulating expression of genes/proteins favoring altered APP processing and enhanced Aβ clearance leading to reduced Aβ plaque deposition, neuroinflammation and cognitive deficits. Overall, this suggests a role for 82-kDa ChAT in AD-like pathology, confirms its gene-regulatory role and highlights it as a potential regulator of neurodegenerative axes, including inflammation, lipid metabolism and insulin pathways.

Materials and methods

Animals, breeding, and experimental design

All experimental procedures were approved by the Committee for the Care and Use of Laboratory Animals at University of Western Ontario, London, Canada. Mice were housed in groups of 3 under conditions compliant with guidelines of the Canadian Council on Animal Care (22–25 °C, 50% humidity, 12-hour light/dark cycle) with free access to chow and water and provided with environmental enrichments (nestlets, cardboard shavings and amber houses).

Homozygous triple mutant APP knock-in mice carrying the Swedish, Beyreuther/Iberian and Arctic mutations ($APP^{NL\text{-}G\text{-}F/NL\text{-}G\text{-}F}$), developed by Saito et al.[28], were obtained from BrainsCAN Rodent Cognition Research and Innovation Core, University of Western Ontario with permission from RIKEN Bioresource Research Center [signed MTA]. These mice were bred with heterozygous Cre+/82-kDa ChAT + expressing transgenic mice to obtain heterozygous APP knock-in mice ($APP^{NL\text{-}G\text{-}F/WT}$, control mice) and heterozygous crosses expressing both the triple mutant APP and 82-kDa ChAT ($APP^{NL\text{-}G\text{-}F/WT}$ X Cre + ChAT+, experimental mice). Heterozygous $APP^{NL\text{-}G\text{-}F}$ mice exhibit accumulating levels of Aβ plaques, reactive glia, dysfunctional synapses and memory deficits in an age-dependent manner with plaque pathology starting at age 4 months[28]. For genotyping, genomic DNA was isolated from tail clippings using RED-Extract-N-Amp Tissue PCR kit (Sigma-Aldrich, #XNAT-100RXN), according to the manufacturer's instructions, and amplified using primers for the $APP^{WT}/APP^{NL\text{-}G\text{-}F}$ (forward: CCCAGGCGGAACATACAAGT, reverse: TGGAAACTGGGACCACCTCT), Cre (forward: GTCC AATTTACTGACCGTACACC, reverse: GTTATTCGGATCATCAGCTACACC) and 82-kDa ChAT (forward: TGTCTGAGTACTGGCTGAATGAC, reverse: TTGGCACAGTCAGTGGGAATG) transgenes. Amplification products were separated on 2% agarose gels and positive bands at 199, 216, 369 and 700 base pairs indicated the presence of 82-kDa ChAT, APP^{WT}, $APP^{NL\text{-}G\text{-}F}$ and Cre transgenes, respectively (Fig S5). A total of 96 mice were used in these studies and divided across the two genotypes as eight mice/sex/age. Experimental points were set at ages of 6, 12 and 18 months, coinciding with the onset of Alzheimer-like pathology[28]. Mice initially underwent neurobehavioral profiling after which they were euthanized and their brains obtained for biochemical studies. For immunofluorescence, mice were anaesthetized using intraperitoneal (IP) thiopental (100 mg/kg)/xylazine (5 mg/kg) and perfused transcardially with ice-cold 1X PBS followed by 4% paraformaldehyde (PFA) in 1X

PBS. For PCR arrays, immunoblots and ELISAs, mice were euthanized by cervical dislocation, then brains were dissected rapidly on ice to isolate hippocampi and cortices which were flash frozen in liquid nitrogen and stored at -80 °C until further processing.

Neurobehavioral studies

At each experimental age, $APP^{NL\text{-}G\text{-}F/WT}$ (control mice) and $APP^{NL\text{-}G\text{-}F/WT}$ X Cre + ChAT+ (experimental mice) mice underwent behavioral testing on a series of tasks. Groups of 16 naïve mice (8 males and 8 females for each genotype), were transferred to the behaviour testing facility at ages 5.5, 11.5 and 17.5 months, prior to when testing began at ages 6, 12 and 18 months of age, respectively. Over 5 weeks, behavior tests were conducted between 9:00 am and 12:00 pm beginning with the open field test, followed by the grip force strength test, Barnes maze and finally Morris water maze. In each of the studies, mice were brought into the testing room 30 min prior to the start of the test with the experimenter blinded to the genotypes of mice. Data were collected and analyzed from males and females independently to assess potential sex-dependent variations.

Habituation and general activity

Habituation learning and general/exploratory behavior were assessed by placing mice in locomotor chambers (20 cm x 20 cm x 30 cm) fitted with an array of infra-red beams to measure activity along x, y and z axes. Data were analyzed using VersaMax 2.0 Fusion software (Accuscan Instruments, Inc., Columbus, OH, USA). Distance travelled and time spent at the margins and center of the field were recorded over 36 sessions, with each session being 10 min in duration and divided equally across three days. Activity collected during the first session and across all 36 sessions was used to assess general/exploratory behavior and habituation learning, respectively.

Weight and force

At 24–48 h after the last session in the locomotor chambers, mice were weighed and their forelimb force assessed using a digital force gauge. Each mouse conducted five trials over a period of 30 min and the average force (N) was normalized to the weight (Kg) to determine the forelimb grip strength (N/Kg).

Learning and memory

To assess hippocampal-dependent spatial learning and memory, we utilized standard versions of a dry maze (Barnes maze) and a wet maze (Morris water maze) with four distinct visual cues spaced evenly around the room. Animal cohorts were divided in two counterbalanced groups assigned opposite target holes/quadrants to offset potential positional effects. Each maze protocol included a training phase to assess learning (16 sessions divided over four days with an inter-trial interval of at least 15 min), and two probe trials conducted one and seven days after the last training sessions to evaluate short- and long-term reference memory, respectively. Anymaze video tracking software (Stoelting; https://stoeltingco.com/Neuroscience/ANY-maze-Video-Tracking-Software~9825) was used to record and analyze both training and probe sessions in both mazes.

Barnes maze

The maze consisted of 20 escape holes distributed equally across a circular white flat platform (92 cm diameter at 105 cm above ground). At the start of each trial, a mouse was placed in an opaque cylindrical chamber that was removed 10 s later with the onset of the aversive stimulus (loud noise/buzzer). The maze was cleaned with 70% ethanol to remove odor clues at the end of each session. Prior to training sessions, mice were adapted to the maze by free exploration for 3 min and being guided to the target location where they remained for 2 min. During the training phase, a trial was terminated when the mouse escaped into the target hole or after three min had elapsed at which time the mouse was guided to the target location and kept there for one min. The training session parameters assessed included total number of errors prior to visiting the target hole (primary errors) and time elapsed until the first target visit/entry (escape latency). For the probe phase, the escape hole was closed and the frequency and duration spent at the target and non-target holes was monitored for 90 s.

Morris water maze

The apparatus included a circular tank (1.2 × 0.5 m) that was 80% filled with water (20 °C ± 2 °C) and a submerged escape platform (10 cm diameter at 1.5 cm below water surface) located at the center of one of four virtual quadrants; northeast, northwest, southeast, and southwest. During training, starting locations were randomized for each trial and at the end of the trial mice were allowed to dry in individual cages. A training trial was terminated when the mouse found the escape platform or after 90 s where the mouse was placed on the platform for 30 s. Total distance, speed and time required to locate the target (escape latency) were recorded for each session. Probe trials were conducted by removing the escape platform and monitoring the swim pattern/duration of the mice for 60 s, starting at a position opposite to the target quadrant.

PCR arrays

We performed two different RT2 Profiler™ PCR Arrays (Qiagen/GeneGlobe), Alzheimer's disease (#PAMM-057ZD) and Cytokines and Chemokines (# PAMM-150ZD). Each array probes 84 pathway-related genes, 5 housekeeping reference genes (Actb, B2m, Gapdh, Gusb, Hsp90ab1), 1 mouse genomic DNA contamination control, 3 reverse transcription controls (to check reverse transcription efficiency) and 3 PCR positive controls (to assess array reproducibility). Arrays were performed on hippocampi from 6 month old mice with 3 independent replicates for each sex and genotype. Tissues were homogenized with a hand-held homogenizer and total RNA was extracted using the RNeasy Plus Mini Kit (Qiagen, #74134). To synthesize cDNA, 0.5 µg RNA was reversed transcribed using the RT2 First Strand Kit (Qiagen, #330404) and the RNase-Free DNase kit (Qiagen, #79254) was used to eliminate genomic DNA contamination. PCR reactions were performed using

the RT2 SYBR Green qPCR mastermix (Qiagen, #330503) and RT2 Profiler™ PCR array plates according to manufacturer's instructions and run on a BioRad CFX Connect System. Analysis of gene expression data was performed using Qiagen's online platform (RT2 Profiler PCR Arrays & Assays Data Analysis software) (https://geneglobe.qiagen.com/ca/analyze). All genes were normalized to a minimum of three reference genes. Data showing at least a two-fold change with a $p \leq 0.05$ were considered significant.

Immnoblots

Cortical and hippocampal protein lysates were prepared by sonicating tissues in N-PER™ Neuronal Protein Extraction Reagent (Thermo, #87792) at a ratio 1:7.5, supplemented with protease (Complete™, Mini Protease Inhibitor Cocktail, tablets, Thomas Scientific, # QZY-04693124001) and phosphatase inhibitors (Phosstop™ tablets, Roche, # 04906837001). Lysates were incubated at 4 °C for 1 h on a rotator after which insoluble debris was sedimented by centrifuging at 14,000 rpm for 15 min at 4 °C. The supernatant was decanted into new tubes and total protein concentrations were measured using Pierce BCA Protein assay kit (Thermo, 23225) with bovine serum albumin as the standard. Proteins were denatured by heating at 95 °C for 10 min in Laemmli's buffer (2% SDS, 10% glycerol, 0.1 M sodium phosphate buffer, pH 7.2, 0.001% bromophenol blue and 2.5% β-mercaptoethanol). An equal amount of protein (25 µg) was loaded and separated on 8% or 12% SDS-PAGE gels and transferred using wet transfer method (transfer buffer: 48 mM Tris, 39 mM glycine, 20% methanol) to polyvinylidene fluoride (PVDF) membranes. Blots were blocked in 5% non-fat dry milk or 5% normal goat serum in 1x Tris-buffered saline (TBS; 50 mM Tris-HCl, 150 mM NaCl, pH 7.4) with 0.1% Tween-20 (0.1% TBST) for 1 h at room temperature, then incubated with primary antibodies diluted in the same blocking buffer overnight at 4 °C. On day two, blots were washed using 0.1% TBST and incubated in secondary antibodies against either mouse or rabbit diluted in the blocking buffer (1:5000-1:10000) for 1 h at room temperature. BioRad's Clarity Western ECL substrate (BioRad, #1705061) was used to detect immunoreactive bands which were imaged using a Chemidoc. imaging system. Densitometric analysis was performed on immunoreactive bands using Image Lab software (BioRad; https://www.bio-rad.com/en-ca/product/image-lab-software?ID=KRE6P5E8Z) and normalized to the loading control β-actin. A list of all the primary and secondary antibodies used in these immunoblots is in Table 1.

Antibody	Vendor/catalogue No.	Dilution for immunoblots	Dilution for immunohistochemistry
Primary antibodies			
Custom Rabbit Anti-82 kDa ChAT (N-terminus, NTab)[35]	GeneMed Synthesis	–	1:100
Rabbit Anti-Iba1	Abcam ab178846	1:1000	1:1000
Mouse Anti-NeuN (clone A60) AlexaFluor 488 Conjugate	Millipore-Sigma Mab377X	–	1:1000
Rabbit Anti-iNOS	Thermo Scientific PA1-036	1:1000	–
Mouse Anti-Cluster differentiation 86 (CD86)	Thermo Scientific MA515697	1:1000	–
Rabbit Anti-Cluster differentiation 206 (CD206)	Abcam ab125028	1:1000	–
Rabbit Anti-Arg1	Proteintech 16001-1-AP	1:1000	–
β-Actin	Millipore-Sigma a5441	1:1000	–
Rabbit Anti-ABCA1	Thermo Scientific PA1-16789	1:1000	–
Rabbit Anti-Insulin degrading enzyme	Abcam ab32216	1:1000	–
Rabbit Anti-LRP1	Abcam ab92544	1:1000	–
Mouse Anti-Aβ	Novus Biologicals NBP2-13075	–	1:1000
Secondary antibodies			
Goat anti Mouse IgG (H + L) Secondary Antibody, Alexa Fluor 568	Invitrogen A11031	–	1:500/1:1000
Goat anti-Rabbit IgG (H + L) Cross-Adsorbed Secondary antibody, Alexa Fluor 488	Invitrogen A11008	–	1:500/1:1000
Goat anti-Rabbit IgG (H + L) Highly Cross-Adsorbed Alexa Fluor 568	Invitrogen A11036	–	1:500/1:1000
HRP-conjugated Goat Anti-Rabbit IgG (H + L)	BioRad 170–6515	1:5000/1:10000	–
HRP-conjugated Goat Anti-Mouse IgG (H + L)	Jackson ImmunoResearch 115-035-003	1:5000/1:10000	–

Table 1. Antibodies: primary and secondary antibodies used for immunoblots and immunofluorescence and their respective dilutions.

Immunohistochemistry and imaging

Perfusion-fixed brains were collected and post-fixed in 4% PFA 1X PBS at 4 °C for 24 h. Subsequently, brains were transferred to 30% sucrose in 1X PBS at 4 °C for 48–72 h for cryoprotection. The brains were then embedded in Tissue-Plus™ O.C.T. Compound (Thermo, #23-730-571), frozen using dry ice, and stored at -80 °C until sectioning. Frozen brains were sectioned using a Leica CM350 cryostat into 40 µm free-floating coronal sections collected in 1X PBS. Sections were transferred into an antigen preserving solution (1% polyvinylpyrrolidone; PVP, 50% ethylene glycol, 1X PBS) and stored at -20 °C until further processing. Briefly, sections were washed with 1X TBS for 1 h to remove excess OCT compound, permeabilized for 10 min in 100% methanol at -20 °C, rinsed with 1X TBS and blocked in 4% normal donkey serum (Abcam, #ab7475) in 1X TBS with 0.05% Triton X-100 for 1 to 2 h at room temperature on a shaker. Afterwards, they were incubated with primary antibodies (Table 1) diluted in 2% normal donkey serum in 1X TBS with 0.05% Triton X-100 overnight on a shaker at room temperature. The next day, sections were washed with 1X TBS to remove excess primary antibody and incubated with corresponding secondary antibodies (Table 1) in 2% normal donkey serum in 1X TBS with 0.05% Triton X-100 for 2 h on a shaker at room temperature. Lastly, sections were rinsed with 1X TBS, mounted on Superfrost plus-charged slides (Thermo Scientific, #12-550-15), air dried and cover slipped with Vectashield hardset mounting medium with DAPI (Vectashield, #VECTH1500). Tiled whole brain scans were acquired using Thermo-Evos imaging system at 20X (dry) magnification while higher resolution fields were obtained on a Leica-TSC SP8 confocal microscope using a 10X (dry) or 40X (oil immersion) objectives with a z-stack step size of 1–4 µm. Image acquisition parameters, within a single experiment, were maintained constant across the experimental groups investigated. Image processing and analysis were performed using Leica Applications Suite (LAS X) and Image J, and analysis was based on three sections per mouse with a minimum acquisition of three to six different fields. The fluorescence-positive area was determined using Image J 1.53 C software and Leica Application Suite X 3.7.4 (https://www.leica-microsystems.com/products/microscope-software/p/leica-las-x-ls/), following thresholding and background subtraction, with consistent analysis parameters across the test groups.

ELISA

Total $A\beta_{1-42}$ was measured in hippocampi harvested from mice aged 6, 12 and 18 months, using the Amyloid beta 42 Human ELISA Kit (ThermoFisher, #KHB3442). Frozen hippocampi were homogenized in 8X volume of cold 5 M guanidine-HCL (50 mM, pH 8.0) using a hand-held homogenizer and incubated on a rotor for 4 h at room temperature. Homogenates were then diluted with N-PER™ Neuronal Protein Extraction Reagent (Thermo, #87792) at a ratio 1:5, supplemented with protease (Complete™, Mini Protease Inhibitor Cocktail, tablets, Thomas Scientific, # QZY-04693124001) and phosphatase inhibitors (Phosstop™ tablets, Roche, # 04906837001) then centrifuged at 16,000xg for 20 min at 4°C. Supernatants were transferred to new tubes and total protein measured by Pierce BCA Protein assay kit (Thermo, #23225) with bovine serum albumin as standard. Prior to the ELISA, samples were diluted using the standard diluent in the kit as follows: 6 months (1:100), 12 months (1:2000) and 18 months (1:4000). The assay was performed according to manufacturer's instructions on a microtiter plate reader (SpectraMax M5, Molecular Devices) at 450 nm and final $A\beta_{1-42}$ levels were normalized to total protein concentrations of the samples.

Statistical analysis

Data analysis was performed using GraphPad Prism software version 9 (https://www.graphpad.com/updates/prism-900-release-notes) and is presented as mean ± standard error of the mean (SEM), unless specified otherwise. Densitometric and immunofluorescence quantifications were analyzed using Student's unpaired t-test, one-way or two-way ANOVA with Sidak's post-hoc test. For behavioral data, statistical significance was assessed using one-way or two-way ANOVA with Sidak's post-hoc test, or two-way RM ANOVA with Tukey's post-hoc test. Sample sizes, reported as n/genotype/sex/age for the different experiments were: 3 for PCR arrays, 4–6 for immunofluorescence/immunoblot experiments and 8 for behavioral experiments. All measurements were compared between genotypes and within genotypes across both sexes and different ages. Statistical significance was set at $p \leq 0.05$.

Data availability

Data sets generated and analyzed during the current study are available from the corresponding author on reasonable request.

Received: 9 April 2024; Accepted: 4 November 2024
Published online: 11 November 2024

References

1. Möller, H. J. & Graeber, M. B. The case described by Alois Alzheimer in 1911. Historical and conceptual perspectives based on the clinical record and neurohistological sections. *Eur. Arch. Psychiatry Clin. NeuroSci.* **248**, 111–122. https://doi.org/10.1007/s004060050027 (1998).
2. Nandi, A. et al. Global and regional projections of the economic burden of Alzheimer's disease and related dementias from 2019 to 2050: a value of statistical life approach. *EClinicalMedicine* **51**, 101580. https://doi.org/10.1016/j.eclinm.2022.101580 (2022).
3. Li, X. et al. Global, regional, and national burden of Alzheimer's disease and other dementias, 1990–2019. *Front. Aging Neurosci.* **14**, 937486. https://doi.org/10.3389/fnagi.2022.937486 (2022).
4. Iqbal, K. et al. Mechanisms of neurofibrillary degeneration and the formation of neurofibrillary tangles. *J. Neural Transm.* **53**, 169–180. https://doi.org/10.1007/978-3-7091-6467-9_15 (1998).
5. Vassar, R. BACE1: the beta-secretase enzyme in Alzheimer's disease. *J. Mol. Neurosci.* **23**(1–2), 105–114. https://doi.org/10.1385/JMN:23:1-2:105 (2004).

6. Liu, P. P., Xie, Y., Meng, X. Y. & Kang, J. S. History and progress of hypotheses and clinical trials for Alzheimer's disease. *Signal. Transduct. Target. Ther.* **4**, 29. https://doi.org/10.1038/s41392-019-0063-8 (2019).
7. Ries, M. & Sastre, M. Mechanisms of Aβ clearance and degradation by glial cells. *Front. Aging Neurosci.* **8**, 160. https://doi.org/10.3389/fnagi.2016.00160 (2016).
8. Saido, T. & Leissring, M. A. Proteolytic degradation of amyloid β-protein. *Cold Spring Harbor Perspect. Med.* **2**(6), a006379. https://doi.org/10.1101/cshperspect.a006379 (2012).
9. Zlokovic, B. V. Neurovascular pathways to neurodegeneration in Alzheimer's disease and other disorders. *Nat. Rev. Neurosci.* **12**(12), 723–738. https://doi.org/10.1038/nrn3114 (2011).
10. Pappolla, M. et al. Evidence for lymphatic Aβ clearance in Alzheimer's transgenic mice. *Neurobiol. Dis.* **71**, 215–219. https://doi.org/10.1016/j.nbd.2014.07.012 (2014).
11. Hong, L., Huang, H. C. & Jiang, Z. F. Relationship between amyloid-beta and the ubiquitin-proteasome system in Alzheimer's disease. *Neurol. Res.* **36**(3), 276–282. https://doi.org/10.1179/1743132813Y.0000000288 (2014).
12. Zhang, Y. D. & Zhao, J. J. TFEB participates in the Aβ-induced pathogenesis of Alzheimer's disease by regulating the autophagy-lysosome pathway. *DNA Cell Biol.* **34**(11), 661–668. https://doi.org/10.1089/dna.2014.2738 (2015).
13. Kurz, A. & Perneczky, R. Amyloid clearance as a treatment target against Alzheimer's disease. *J. Alzheimer's Dis.* **24**, 61–73. https://doi.org/10.3233/JAD-2011-102139 (2011).
14. Tokuda, T. et al. Lipidation of apolipoprotein E influences its isoform-specific interaction with Alzheimer's amyloid beta peptides. *Biochem. J.* **2**(Pt 2), 359–365 (2000).
15. Jiang, Q. et al. ApoE promotes the proteolytic degradation of Abeta. *Neuron* **58**(5), 681–693. https://doi.org/10.1016/j.neuron.2008.04.010 (2008).
16. Laporte, V. et al. Uptake of Abeta 1-40- and abeta 1-42-coated yeast by microglial cells: a role for LRP. *J. Leukoc. Biol.* **76**(2), 451–461. https://doi.org/10.1189/jlb.1203620 (2004).
17. Sagare, A. P. et al. Pericyte loss influences Alzheimer-like neurodegeneration in mice. *Nat. Commun.* **4**, 2932. https://doi.org/10.1038/ncomms3932 (2013).
18. Kar, S., Slowikowski, S. P., Westaway, D. & Mount, H. T. Interactions between beta-amyloid and central cholinergic neurons: implications for Alzheimer's disease. *J. Psychiatry Neurosci.* **29**(6), 427–441 (2004).
19. Takata, K. et al. Galantamine-induced amyloid-{beta} clearance mediated via stimulation of microglial nicotinic acetylcholine receptors. *J. Biol. Chem.* **285**(51), 40180–40191. https://doi.org/10.1074/jbc.M110.142356 (2010).
20. Schliebs, R. Basal forebrain cholinergic dysfunction in Alzheimer's disease–interrelationship with beta-amyloid, inflammation and neurotrophin signaling. *Neurochem. Res.* **30**(6–7), 895–908. https://doi.org/10.1007/s11064-005-6962-9 (2005).
21. McKinney, M. & Jacksonville, M. C. Brain cholinergic vulnerability: relevance to behavior and disease. *Biochem. Pharmacol.* **70**(8), 1115–1124. https://doi.org/10.1016/j.bcp.2005.05.019 (2005).
22. Beach, T. G. et al. The cholinergic deficit coincides with Abeta deposition at the earliest histopathologic stages of Alzheimer disease. *J. Neuropathol. Exp. Neurol.* **59**(4), 308–313. https://doi.org/10.1093/jnen/59.4.308 (2000).
23. Resendes, M. C., Dobransky, T., Ferguson, S. S. & Rylett, R. J. Nuclear localization of the 82-kDa form of human choline acetyltransferase. *J. Biol. Chem.* **274**(27), 19417–19421. https://doi.org/10.1074/jbc.274.27.19417 (1999).
24. Gill, S. K. et al. 82-kDa choline acetyltransferase is in nuclei of cholinergic neurons in human CNS and altered in aging and Alzheimer disease. *Neurobiol. Aging* **28**(7), 1028–1040. https://doi.org/10.1016/j.neurobiolaging.2006.05.011 (2007).
25. Albers, S. et al. Nuclear 82-kDa choline acetyltransferase decreases amyloidogenic APP metabolism in neurons from APP/PS1 transgenic mice. *Neurobiol. Dis.* **69**, 32–42. https://doi.org/10.1016/j.nbd.2014.05.008 (2014).
26. Winick-Ng, W. et al. 82-kDa choline acetyltransferase and SATB1 localize to β-amyloid induced matrix attachment regions. *Sci. Rep.* **6**, 23914. https://doi.org/10.1038/srep23914 (2016).
27. AlQot, H. E. & Rylett, R. J. A novel transgenic mouse model expressing primate-specific nuclear choline acetyltransferase: insights into potential cholinergic vulnerability. *Sci. Rep.* **13**(1), 3037. https://doi.org/10.1038/s41598-023-30155-4 (2023).
28. Saito, T. et al. Single app knock-in mouse models of Alzheimer's disease. *Nat. Neurosci.* **17**(5), 661–663. https://doi.org/10.1038/nn.3697 (2014).
29. Solito, E. & Sastre, M. Microglia function in Alzheimer's disease. *Front. Pharmacol.* **3**, 14. https://doi.org/10.3389/fphar.2012.00014 (2012).
30. Selkoe, D. J. Alzheimer's disease results from the cerebral accumulation and cytotoxicity of amyloid beta-protein. *J. Alzheimers Dis.* **3**(1), 75–80. https://doi.org/10.3233/jad-2001-3111 (2001).
31. Rivera, E. J. et al. Insulin and insulin-like growth factor expression and function deteriorate with progression of Alzheimer's disease: link to brain reductions in acetylcholine. *J. Alzheimers Dis.* **8**(3), 247–268. https://doi.org/10.3233/jad-2005-8304 (2005).
32. Campos-Peña, V. et al. Amyloid β, lipid metabolism, basal cholinergic system, and therapeutics in Alzheimer's disease. *Int. J. Mol. Sci.* **23**(20), 12092. https://doi.org/10.3390/ijms232012092 (2022).
33. Nonner, D., Panickar, K., Barrett, E. F. & Barrett, J. N. Bone morphogenetic proteins and neurotrophins provide complementary protection of septal cholinergic function during phosphatase inhibitor-induced stress. *J. Neurochem.* **91**(1), 77–87. https://doi.org/10.1111/j.1471-4159.2004.02687.x (2004).
34. Trettel, F., Di Castro, M. A. & Limatola, C. Chemokines: key molecules that orchestrate communication among neurons, microglia and astrocytes to preserve brain function. *Neuroscience* **439**, 230–240. https://doi.org/10.1016/j.neuroscience.2019.07.035 (2020).
35. Koldamova, R. P. et al. 22R-hydroxycholesterol and 9-cis-retinoic acid induce ATP-binding cassette transporter A1 expression and cholesterol efflux in brain cells and decrease amyloid beta secretion. *J. Biol. Chem.* **278**(15), 13244–13256. https://doi.org/10.1074/jbc.M300044200 (2003).
36. Holtzman, D. M. et al. Expression of human apolipoprotein E reduces amyloid-beta deposition in a mouse model of Alzheimer's disease. *J. Clin. Investig.* **103**(6), R15–R21. https://doi.org/10.1172/JCI6179 (1999).
37. Kanekiyo, T. & Bu, G. The low-density lipoprotein receptor-related protein 1 and amyloid-β clearance in Alzheimer's disease. *Front. Aging Neurosci.* **6**, 93. https://doi.org/10.3389/fnagi.2014.00093 (2014).
38. Fan, Z., Brooks, D. J., Okello, A. & Edison, P. An early and late peak in microglial activation in Alzheimer's disease trajectory. *Brain* **140**(3), 792–803. https://doi.org/10.1093/brain/aww349 (2017).
39. Wang, Q. et al. Microglia polarization in Alzheimer's disease: mechanisms and a potential therapeutic target. *Front. Aging Neurosci.* **13**, 772717. https://doi.org/10.3389/fnagi.2021.772717 (2021).
40. Jurga, A. M., Paleczna, M. & Kuter, K. Z. Overview of general and discriminating markers of differential microglia phenotypes. *Front. Cell. Neurosci.* **14**, 198. https://doi.org/10.3389/fncel.2020.00198 (2020).
41. Browne, T. C. et al. IFN-γ production by amyloid β-specific Th1 cells promotes microglial activation and increases plaque burden in a mouse model of Alzheimer's disease. *J. Immunol.* **190**(5), 2241–2251. https://doi.org/10.4049/jimmunol.1200947 (2013).
42. Taylor, R. A. et al. TGF-β1 modulates microglial phenotype and promotes recovery after intracerebral hemorrhage. *J. Clin. Investig.* **127**(1), 280–292. https://doi.org/10.1172/JCI88647 (2017).
43. Lepore, F. et al. CXCL16/CXCR6 axis drives microglia/macrophages phenotype in physiological conditions and plays a crucial role in glioma. *Front. Immunol.* **9**, 2750. https://doi.org/10.3389/fimmu.2018.02750 (2018).
44. Nguyen, T. V. et al. Small molecule p75NTR ligands reduce pathological phosphorylation and misfolding of tau, inflammatory changes, cholinergic degeneration, and cognitive deficits in AβPP(L/S) transgenic mice. *J. Alzheimers Dis.* **42**(2), 459–483. https://doi.org/10.3233/JAD-140036 (2014).

45. Guan, Y. Z. et al. Nicotine inhibits microglial proliferation and is neuroprotective in global ischemia rats. *Mol. Neurobiol.* **51**(3), 1480–1488. https://doi.org/10.1007/s12035-014-8825-3 (2015).
46. Liu, Q. et al. α7 nicotinic acetylcholine receptor-mediated anti-inflammatory effect in a chronic migraine rat model via the attenuation of glial cell activation. *J. Pain Res.* **11**, 1129–1140. https://doi.org/10.2147/JPR.S159146 (2018).
47. Jans, D. A. & Hübner, S. Regulation of protein transport to the nucleus: central role of phosphorylation. *Physiol. Rev.* **76**, 651–685. https://doi.org/10.1152/physrev.1996.76.3.651 (1996).
48. Dobransky, T., Davis, W. L., Xiao, G. H. & Rylett, R. J. Expression, purification and characterization of recombinant human choline acetyltransferase: phosphorylation of the enzyme regulates catalytic activity. *Biochem. J.* **349**, 141–151. https://doi.org/10.1042/0264-6021:3490141 (2000).
49. Latif-Hernandez, A. et al. Subtle behavioral changes and increased prefrontal-hippocampal network synchronicity in APPNL-G-F mice before prominent plaque deposition. *Behav. Brain. Res.* **364**, 431–441. https://doi.org/10.1016/j.bbr.2017.11.017 (2019).
50. Whyte, L. S. et al. Reduction in open field activity in the absence of memory deficits in the AppNL-G-F knock-in mouse model of Alzheimer's disease. *Behav. Brain. Res.* **336**, 177–181. https://doi.org/10.1016/j.bbr.2017.09.006 (2018).
51. Wang, S. et al. Age-dependent behavioral and metabolic assessment of AppNL-G-F/NL-G-F knock-in (KI) mice. *Front. Mol. Neurosci.* **15**, 909989. https://doi.org/10.3389/fnmol.2022.909989 (2022).
52. Locci, A. et al. Comparison of memory, affective behavior, and neuropathology in APPNLGF knock-in mice to 5xFAD and APP/PS1 mice. *Behav. Brain. Res.* **404**, 113192. https://doi.org/10.1016/j.bbr.2021.113192 (2021).
53. Pervolaraki, E. et al. Insoluble Aβ overexpression in an app knock-in mouse model alters microstructure and gamma oscillations in the prefrontal cortex, affecting anxiety-related behaviours. *Dis. Models Mech. Int. J. Dev. Neurosci.* **1221**(97), 040550. https://doi.org/10.1242/dmm.040550 (20192003).
54. Klingner, M. et al. Alterations in cholinergic and non-cholinergic neurotransmitter receptor densities in transgenic Tg2576 mouse brain with beta-amyloid plaque pathology. *Int. J.Dev. Neurosci.* **21**(7), 357–369. https://doi.org/10.1016/j.ijdevneu.2003.08.001 (2003).
55. Mehla, J. et al. Age-dependent behavioral and biochemical characterization of single APP knock-in mouse (APPNL-G-F/NL-G-F) model of Alzheimer's disease. *Neurobiol. Aging* **75**, 25–37. https://doi.org/10.1016/j.neurobiolaging.2018.10.026 (2019).
56. Nieraad, H. et al. Impact of hyperhomocysteinemia and different dietary interventions on cognitive performance in a knock-in mouse model for Alzheimer's disease. *Nutrients* **12**(11), 3248. https://doi.org/10.3390/nu12113248 (2020).
57. Sakakibara, Y., Sekiya, M., Saito, T., Saido, T. C. & Iijima, K. M. Cognitive and emotional alterations in app knock-in mouse models of Aβ amyloidosis. *BMC Neurosci.* **19**(1), 46. https://doi.org/10.1186/s12868-018-0446-8 (2018).
58. Taglialatela, G., Hogan, D., Zhang, W. R. & Dineley, K. T. Intermediate- and long-term recognition memory deficits in Tg2576 mice are reversed with acute calcineurin inhibition. *Behav. Brain. Res.* **200**(1), 95–99. https://doi.org/10.1016/j.bbr.2008.12.034 (2009).
59. Arendash, G. W. et al. Progressive, age-related behavioral impairments in transgenic mice carrying both mutant amyloid precursor protein and presenilin-1 transgenes. *Brain Res.* **891**(1–2), 42–53. https://doi.org/10.1016/s0006-8993(00)03186-3 (2001).
60. Mielke, M. M., Vemuri, P. & Rocca, W. A. Clinical epidemiology of Alzheimer's disease: assessing sex and gender differences. *Clin. Epidemiol.* **6**, 37–48. https://doi.org/10.2147/CLEP.S37929 (2014).
61. Puzzo, D., Lee, L., Palmeri, A., Calabrese, G. & Arancio, O. Behavioral assays with mouse models of Alzheimer's disease: practical considerations and guidelines. *Biochem. Pharmacol.* **88**(4), 450–467. https://doi.org/10.1016/j.bcp.2014.01.011 (2014).
62. Matsuo, A. et al. Rat choline acetyltransferase of the peripheral type differs from that of the common type in intracellular translocation. *Neurochem. Int.* **46**, 423–433. https://doi.org/10.1016/j.neuint.2004.11.006 (2005).
63. Iatrou, A., Clark, E. M. & Wang, Y. Nuclear dynamics and stress responses in Alzheimer's disease. *Mol. Neurodegener.* **16**(1), 65. https://doi.org/10.1186/s13024-021-00489-6 (2021).
64. Ramsey, C. P. et al. Expression of Nrf2 in neurodegenerative diseases. *J. Neuropathol. Exp. Neurol.* **66**(1), 75–85. https://doi.org/10.1097/nen.0b013e31802d6da9 (2007).
65. Mastroeni, D. et al. Reduced RAN expression and disrupted transport between cytoplasm and nucleus; a key event in Alzheimer's disease pathophysiology. *PLoS ONE* **8**(1), e53349. https://doi.org/10.1371/journal.pone.0053349 (2013).
66. Brandscheid, C. et al. Altered gut microbiome composition and tryptic activity of the 5xFAD Alzheimer's mouse model. *J. Alzheimers Dis.* **56**(2), 775–788. https://doi.org/10.3233/JAD-160926 (2017).

Acknowledgements

This research was funded by an operating grant from the Canadian Institutes of Health Research (CIHR) to RJR. HEA was the recipient of a Doctoral Research Award from the Alzheimer Society of Canada. HEA and RJR designed the experiments with HEA carrying out experimental work and data analysis. HEA and RJR interpreted the data and wrote the manuscript. The authors do not have any competing interests in relation to this research.

Author contributions

HEA and RJR designed the experiments, HEA performed the experiments and prepared figures, HEA and RJR wrote and finalized the manuscript. All authors have reviewed the final manuscript.

Declarations

Competing interests

The authors declare no competing interests.

Additional information

Supplementary Information The online version contains supplementary material available at https://doi.org/10.1038/s41598-024-78751-2.

Correspondence and requests for materials should be addressed to R.J.R.